Web-based histology reference atlas for the freshwater crustacean *Daphnia magna*

Short title: Web-based *Daphnia* histology reference atlas

Mee S. Ngu[1,2], Daniel J. Vanselow[1,2], Carolyn R. Zaino[1,2], Alex Y. Lin[1,2], Jean E. Copper[1,2], Margaret J. Beaton[3], John K. Colbourne[4], Keith C. Cheng[1,2,*], Khai C. Ang[1,2,*]

[1]Department of Pathology, Pennsylvania State University College of Medicine, Pennsylvania, USA

[2]Jake Gittlen Laboratories for Cancer Research, Pennsylvania State University College of Medicine, Pennsylvania, USA

[3]Department of Biology, Mount Allison University, Sackville, Canada

[4]School of Biosciences, The University of Birmingham, Birmingham, UK

*Corresponding authors:

Khai C. Ang (kca2@psu.edu)

Keith C. Cheng (kcheng76@gmail.com)

Abstract

Daphnia, an important model system for the study of evolution, development, phenotypic plasticity, and environmental health, lacks a modern reference atlas for microanatomy. To facilitate the comprehensive assessment of phenotypic effects of genes and environment, we created the *Daphnia* histology reference atlas (http://daphnia.io/anatomy/), a tractable, interactive web-based tool that provides insight into normal phenotype through vectorized annotations overlaid onto digital histology sections imaged at 40X magnification. Guided by our expert-curated and multimodal informed hierarchical anatomical ontology, we show that this resource can be used to elucidate sex-specific differences between female and male *Daphnia magna* in each of 3 orthogonal planes, providing new insight for the study of sex-specific traits. This atlas is a new, open-source resource for the *Daphnia* community to facilitate education and research collaboration, and as a precursor for the 3D atlas. It is also our intention that this atlas aids in phenotypic anchoring of large-scale biomolecular (multi-omics) data from comparative toxicological studies. Greater access to high-quality histological data may clarify cross-correlations between microanatomic and multi-omic phenotypes caused by genetic variation, environment, and disease across phylogeny.

Introduction

Keystone species of freshwater ecosystems (algae, zooplankton, fish) forming a food chain, are used in ecotoxicology as sentinels to monitor water quality, manage chemical risks to the environment, and serve as early warning signs of chemical health hazards that can cause human disease (1). *Daphnia*, a branchiopod micro-crustacean, is one of the most abundant zooplankters of lentic ecosystems around the globe and a model system in the fields of ecology and evolution (2,3). *Daphnia magna* primarily inhabit freshwater environments throughout the Northern Hemisphere and South Africa yet are distributed to laboratories around the globe as an established invertebrate model in ecotoxicology. It is sensitive to environmental contaminants, which impact its growth, reproduction, mobility, and mortality (4–6). It has been widely used as an indicator of water quality, assigned a role in setting regulatory criteria for toxicity testing by government agencies worldwide (7–10), and has assumed a central role in ecotoxicogenomics (11,12). Its extensive utilization for toxicological studies makes it important to establish a

comprehensive reference atlas to enable whole-organism phenotyping and characterization of the full range of cellular and molecular phenotypic responses to environmental contaminants.

Histopathology permits the identification of cell- and tissue-specific changes in whole organisms, making it a powerful tool for detecting the adverse effects of toxicants. Multiple histopathology-based toxicological screens using fish (13–15) and aquatic invertebrates (16,17) have been reported. Ideally, the evaluation of toxic effects of chemicals, environmental contaminants, and pollutants identifies all affected cell types and organ systems so that the mechanisms underlying adverse outcomes and disease can be accurately predicted and better understood. However, identification of these toxic effects requires prior knowledge of normal structure, which can be most readily facilitated through atlases in the field of medicine (18) and comparative biology (19). Atlases provide a systematic approach for understanding the anatomical and histological context of all cells and tissues in both normal and diseased states. This systematic approach is more useful and accessible by the research community and the public with the web-based, open-source platform. Web-based reference atlases of various model organisms (e.g., zebrafish at http://bio-atlas.com/zebrafish/, *Caenorhabditis elegans* at www.wormatlas.org, and mouse brain at http://mouse.brain-map.org) are valuable resources and tools for research and education.

With histology as the foundation for understanding normal anatomy, we present a web-based histology reference atlas of *D. magna*. This atlas is an extensive collection of high-resolution virtual slides for both male and female *D. magna* in three orthogonal planes (coronal, sagittal, and transverse), accompanied by a systematic and hierarchically organized anatomical ontology. The interactive viewer of this atlas enables visualization of virtual slides up to 40X magnification and highlighting of anatomical structures with corresponding labels, which allows for quick structure identification. This feature allows visualization and comparison of sexual-dimorphic traits in *Daphnia* reproduced parthenogenetically (20,21). This atlas serves as the foundation for the development of a comprehensive 3D atlas. It will also serve as a foundation for spatial biology to assess the toxicological phenotypic effects of pollutants that complement non-targeted biomolecular approaches, thereby enabling a fuller understanding of the causal links to adversity using sentinel organisms.

Results and discussion

The overall strategy of the *Daphnia* Histology Reference Atlas (DaHRA) involved designing a casting mold to ensure consistency in sample orientation for histology sectioning in any of the three orthogonal orientations, optimizing sample preparation and staining for histology, labeling, and digital segmentation of anatomical structures, and constructing a web interface for the presentation of histological data and annotation (Figure 1).

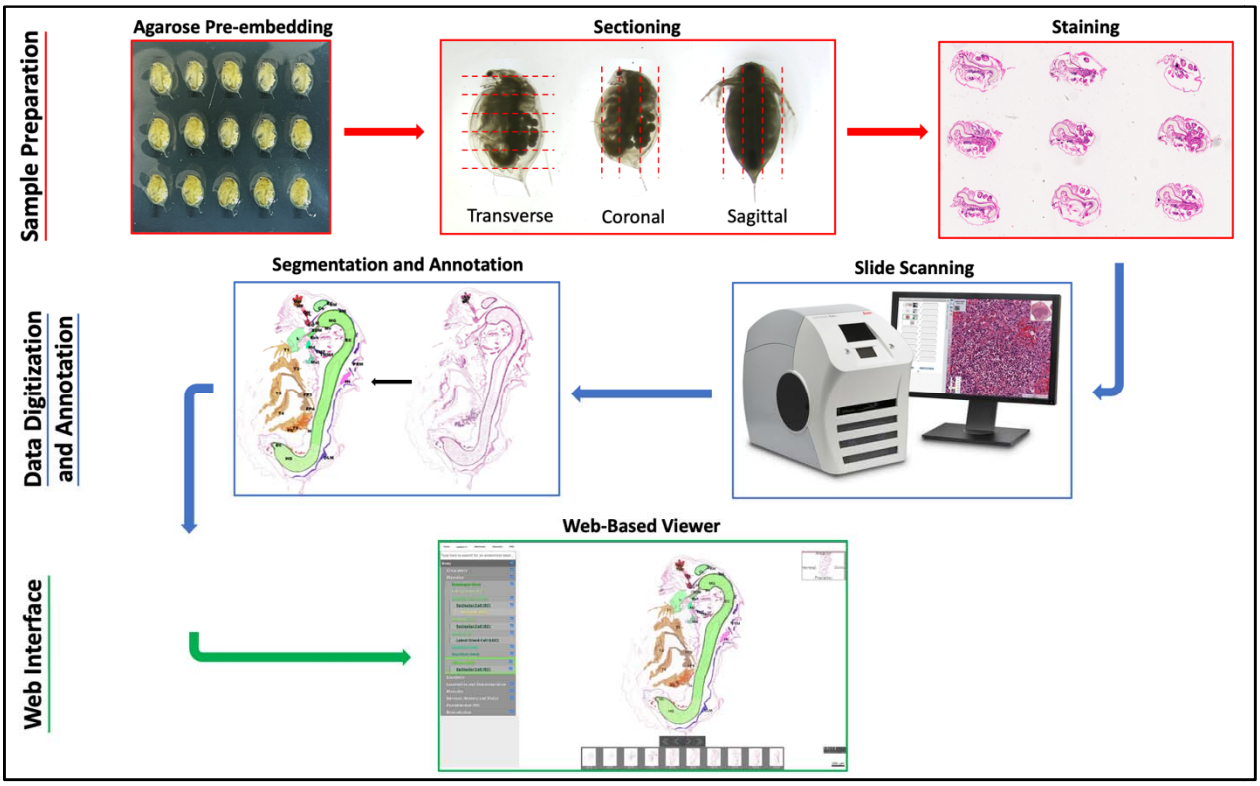

Figure 1. Overview of the strategy for generating DaHRA. Positioning of Bouin's-fixed *Daphnia* samples was facilitated using agarose block cast from a specialized casting mold to achieve near orthogonal alignment for histology sectioning. After processing and sectioning, hematoxylin and eosin-stained slides were digitalized and representative images were selected for labeling and segmentation of anatomical structures. Finally, annotations and virtual images were
presented in the web-based viewer.

Triangle casting mold for agarose pre-embedding

Precise and consistent orientation of samples in paraffin is critical for achieving near orthogonal alignment. To this end, samples were pre-embedded in agarose blocks prior to downstream tissue processing for paraffin embedding. Specialized casting molds were engineered for this study to produce agarose blocks with wells that house individual *Daphnia* samples. Casting molds with three different teeth designs: sloped rectangle, triangle, and rectangle, were tested for efficacy (S1 Fig.). The dimensions of each mold (24 mm X 29 mm) are slightly smaller than the tissue cassettes (27 mm X 31mm) used for tissue processing. Molds were printed using stereolithography (3D-SLA). 3D-SLA printing at 25 µm resolution creates a smooth surface for the mold, allowing the agarose block to be peeled off easily. Spacing of 1 mm between teeth ensured adequate rigidity between wells, while mold thickness of at least 4 mm provided an adequate surface for taping to hold molten agarose. Embedding trials with different casting molds concluded that "triangle mold" with teeth length of 4.5 mm, and height and width of 1.5 mm (Figure 2A-B, STL file in S1 File) allowed precise positioning of *D. magna* samples with ease and yielded consistent orthogonal orientation of histological sections (Figure 2G).

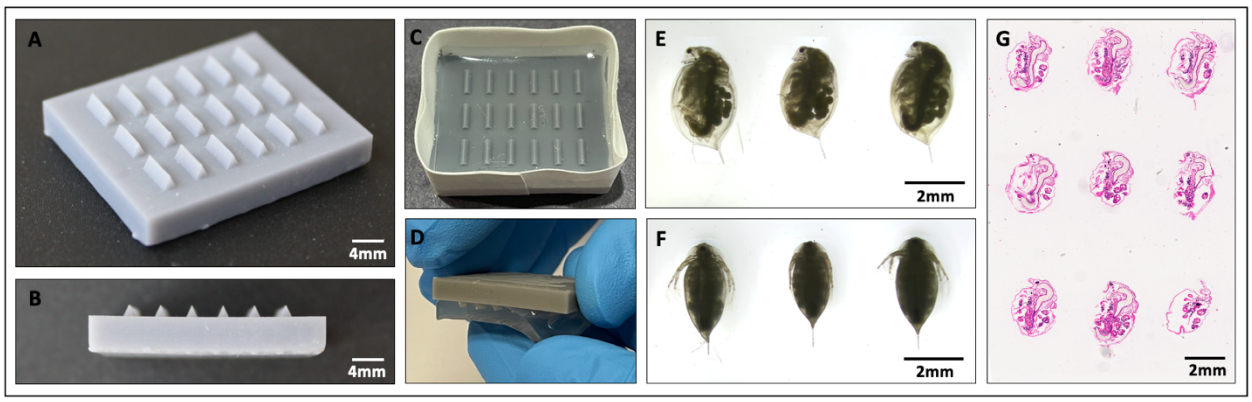

Figure 2. Agarose embedding using casting mold for histological processing. (A) Top view and **(B)** side view of "triangle mold" printed by stereo-lithography (3D-SLA). **(C)** Casting 1% agarose block in the taped mold. **(D)** Agarose block being removed from the mold after solidification by peeling the gel downwards. **(E)** *Daphnia magna* samples were laid on their sides with a swimming antenna in the wells, the rostra facing the same direction for sagittal plane sectioning, and **(F)** laid on their back in the wells for coronal and transverse plane sectioning. **(G)** The histological section showed the position of samples at a similar plane.

Bouin's is a fixative of choice for *Daphnia* histology

The accurate representation of histological microanatomy depends upon the preservation of tissue structure with minimal distortion and optimal staining that allows a clear distinction between different cell types and subcellular structures. Chemical reactions between fixatives and biological tissue result in distortions known as fixation artifacts. To minimize these artifacts, we evaluated the effectiveness of three common fixatives; Bouin's solution, 4% Paraformaldehyde (PFA), and 10% Neutral Buffered Formalin (NBF), and assessed changes in tissue volume and architecture, the extent of tissue preservation, and clarity of cell boundaries. Histology sections of *D. magna* samples fixed with Bouin's solution at room temperature for 48 hours showed the best fixation and nuclear clarity. Preservation by Bouin's solution provided clearer cell boundaries that allowed easier distinction between nerve fibers and cells in the optic lobe (OL) and cerebral ganglion (CG) (Figure 3A). Poor fixation is commonly encountered in the gut, presumably due to the presence of digestive enzymes (22). Bouin's solution resulted in good gut fixation where microvilli were present along the majority of the intestinal lumen and nucleoli in the gut epithelial cells were also more distinct (Figure 3B Inset). Nurse cells and yolk granules were more intact in the ovaries (Figure 3C), and cellular features across the developing embryos are generally more distinct (Figure 3D). Overall, Bouin's solution provided consistent fixation throughout the whole sample and yielded good preservation across tissue and cell types (see S3 Fig. for the result of fixation by 4% PFA and 10% NBF).

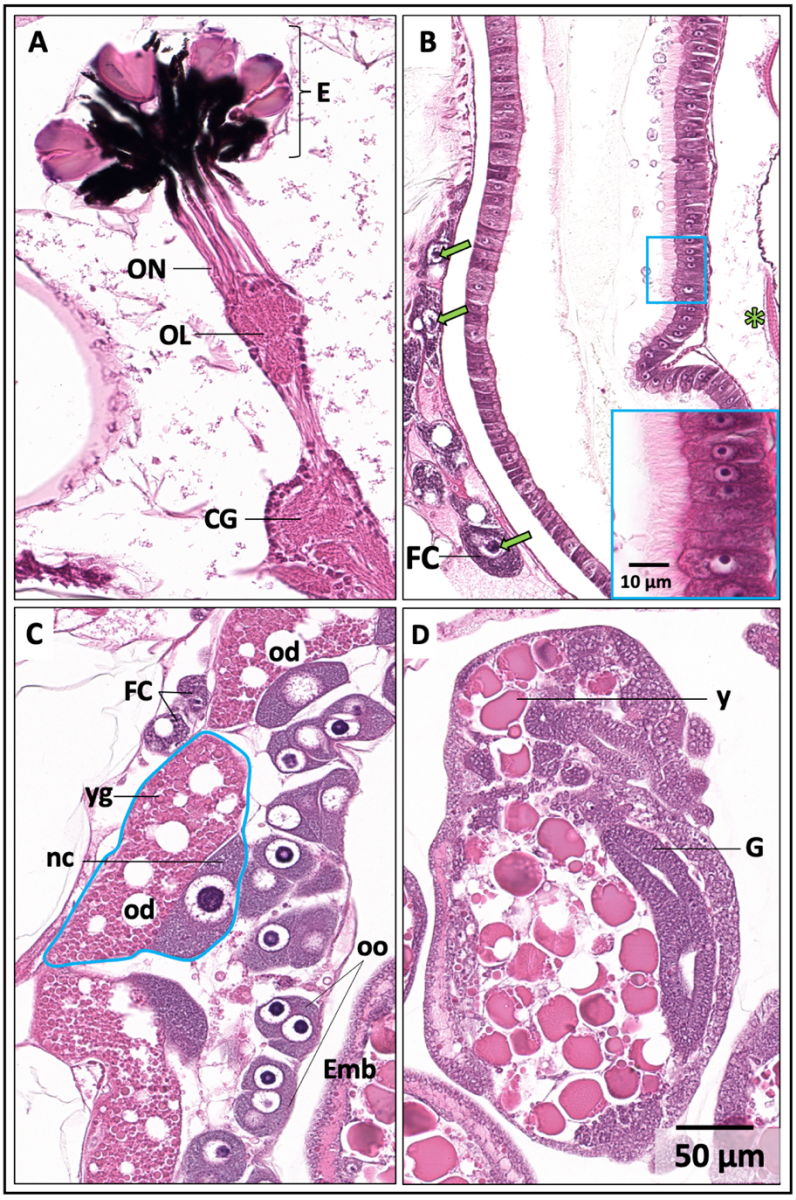

Figure 3. Fixation by Bouin's solution allows visualization of cellular details across anatomical structures: **(A)** nerve fibers and cells in the optic lobe (OL) and cerebral ganglion (CG), **(B)** microvilli and nucleoli of the epithelial cells (inset) in the midgut, nucleoli in the fat cells (FC) (arrows) and muscle striations (asterisk), **(C)** yolk granules (yg) and nurse cell (nc) in an ovarian egg (outlined in blue), and **(D)** developing embryo in the brood chamber. Emb, embryo; G, gut precursor; od, oil droplet; oo, oocytes.

Segmentation of anatomical structures for DaHRA

For each plane, a subset of virtual images derived from one serially sectioned *Daphnia* is selected for the labeling and segmentation of its anatomical structures. The segmentation, accompanied by the anatomical ontology and color-coded based on organ systems (S2 File),

results in interactive color overlays on the atlas. Our anatomical terminology for the ontology is modified from the extensive work of Fryer (1991). To ensure consistency and relevancy of the ontology with current research, we also cross-referenced the extensive work of Fryer (1991) with other published literature (23–49). This systematic review aided our segmentation of each anatomical structure. We also checked for the congruency of each segmented structure in the three orthogonal histology planes. Accurate segmentation of some substructures such as exopodite, epipodite, and endite of the thoracic limbs, is particularly challenging in histology images. To minimize the inaccuracy in annotation, some of the substructures are not labeled individually. To overcome the limitations of histology, we are generating and incorporating 3D data into this atlas to enhance structural and morphological details. We will continue to update this atlas as more images are generated and with feedback from the *Daphnia* scientific community.

Interactive viewer for DaHRA

DaHRA (http://daphnia.io/anatomy/) presents 40X magnification digital scans of ~5 µm thick histological sections generated from serially sectioned *D. magna* of both sexes in three orthogonal planes (coronal, sagittal, and transverse). A viewer was developed to combine digital scans and annotations into a seamless experience to provide user-friendly access to high-resolution data. In the viewer, anatomical ontology is listed on the left, in a hierarchical tree that can be expanded and collapsed (Figure 4). A check in the checkbox indicates that the structure is labeled with a corresponding color overlay. Structures with underlined labels indicate at least one nested substructure (for example, “microvilli” under “epithelial cell”, both under “midgut"). Hovering over a structure dynamically highlights the corresponding structure or structure groups in the viewer, temporarily hiding other checked structures. The search function above the ontology assists in finding the structure in the list.

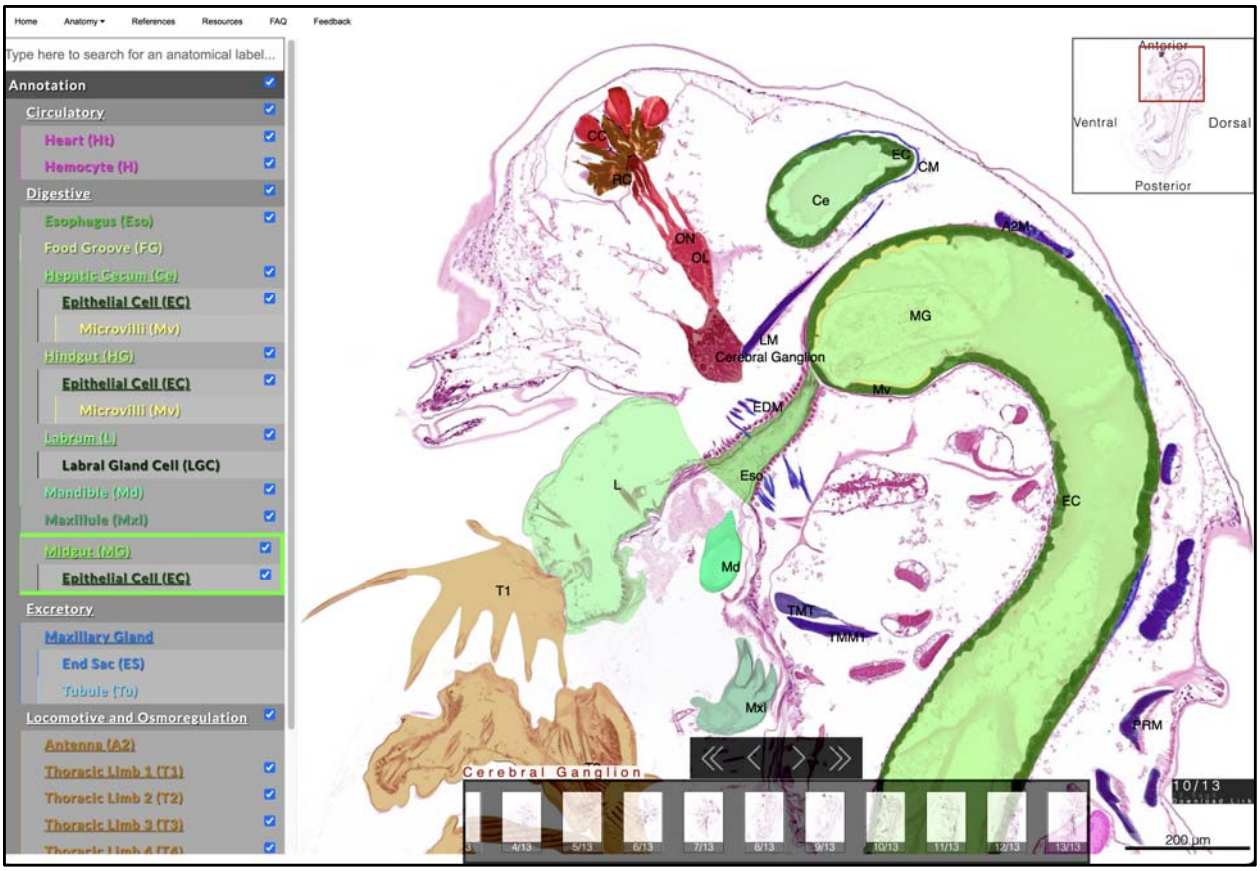

Figure 4. Overview of the interactive web-based viewer for DaHRA. The left pane of the viewer includes an expandable hierarchical tree of anatomical structures; the checked boxes indicate which structures are labeled in the image. The image shows acronym labels; hovering the mouse cursor over an acronym or its corresponding region will bring up the structure's full name. Unchecking a box will eliminate the corresponding color overlay and annotation.

In the image portion of the viewer, all available color overlays and acronym labels are on display by default (indicated by checked checkboxes) (Figure 4). Hovering the mouse cursor over a colored region on the image will display its full name. Clicking on the colored region will change the colored overlay to highlight the border only. While images with interactive highlighting of anatomical structures assist in structure identification, additional unannotated images of serially sectioned *D. magna* are categorized under 'Full Series'. All the files (.ai, tiff, SVG) for exploring the atlas are freely available for download.

A video clip demonstrating the features of the atlas (S 3 File) can be found on the landing page of the atlas (http://daphnia.io/anatomy/). The atlas also contains a list of *Daphnia*-specific

glossary and protocols used in generating this atlas under the “Resource” tab. The “Reference” tab contains a list of published literature used in cross-referencing *Daphnia* anatomy. To enable collaborative effort with the scientific community, keep the atlas relevant to scientific progress and ensure the accuracy of the atlas content, the “Feedback” tab provides a platform for users to leave comments and suggestions.

Daphnia magna anatomy

Daphnia has been the subject of biological and ecological studies (2,30,50). Studies on its functional anatomy, physiology, and development are extensive, however, histology images are not widely available. DaHRA presents the first extensive collection of high-resolution virtual slides of both sexes of *D. magna*, *a* comprehensive visualization platform to interrogate *Daphnia* anatomy. Representative images from each of the three orthogonal planes showing the most anatomical structures of females (Figure 5-7) and males (Figure 8-10) are presented below with a brief description and links to the atlas for the color-overlays.

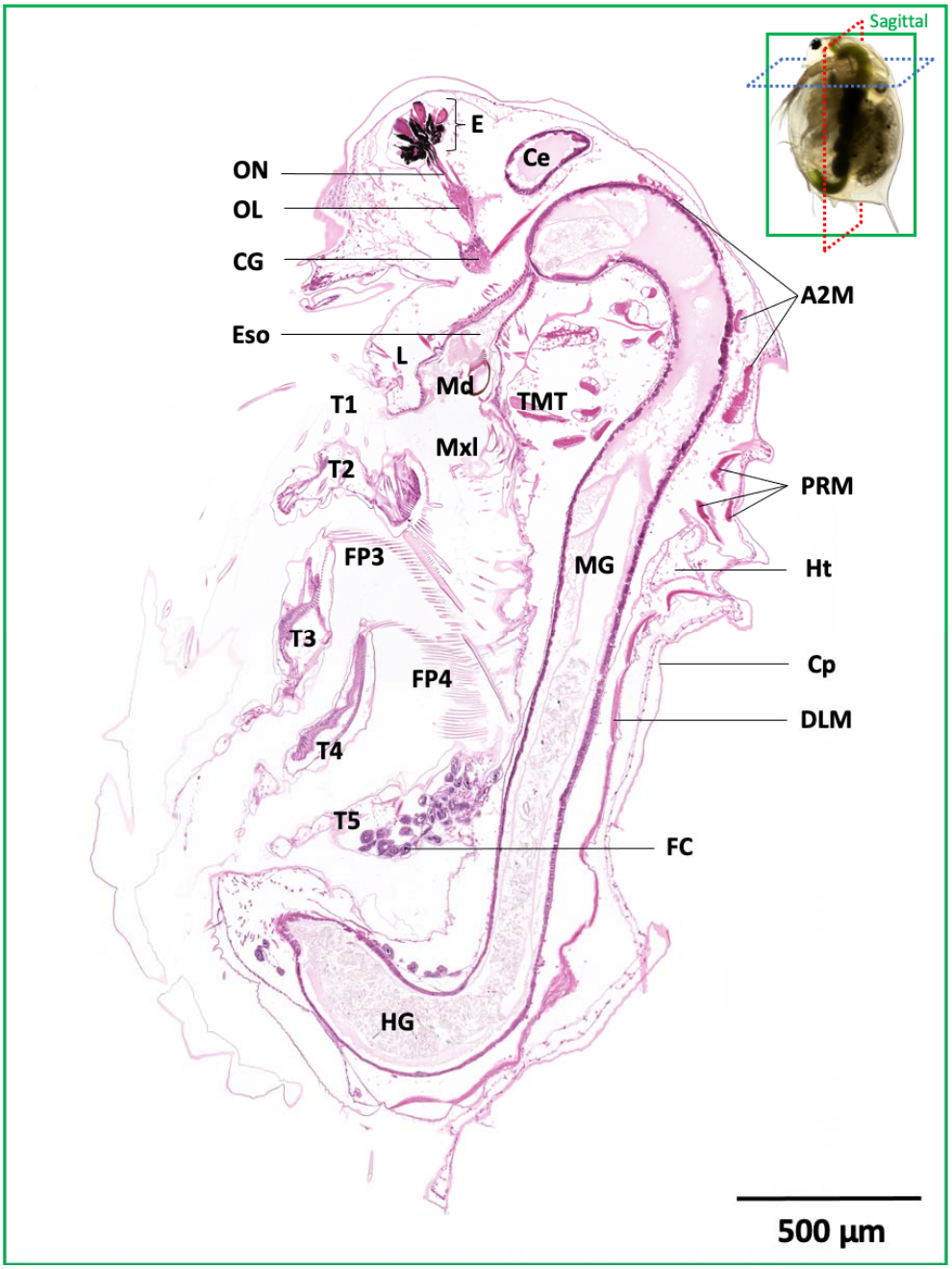

Figure 5. Representative image showing anatomical structures of female *D. magna* in the sagittal plane. The sagittal plane at the approximate median section displays the connection of compound eye (E) to optic lobe (OL) and cerebral ganglion (CG) by optic nerves (ON). The labrum (L), maxillule (Mxl), and mandible (Md) are anterior to the esophagus (Eso) that opens into the midgut (MG) and is followed by the hindgut (HG). This section also cuts through the five thoracic limbs (T1-5) with filter plates (FP3, FP4), the antennal muscles (A2M), the posterior rotator muscle of mandibles (PRM), the heart (Ht), and shows the extent of dorsal longitudinal muscle (DLM) along the gut. Other features seen include the carapace (Cp), hepatic cecum (Ce), fat cells (FC), and transverse mandibular tendon (TMM). Corresponding atlas link: http://daphnia.io/anatomy/histology/?t=sagittal_female&z=10

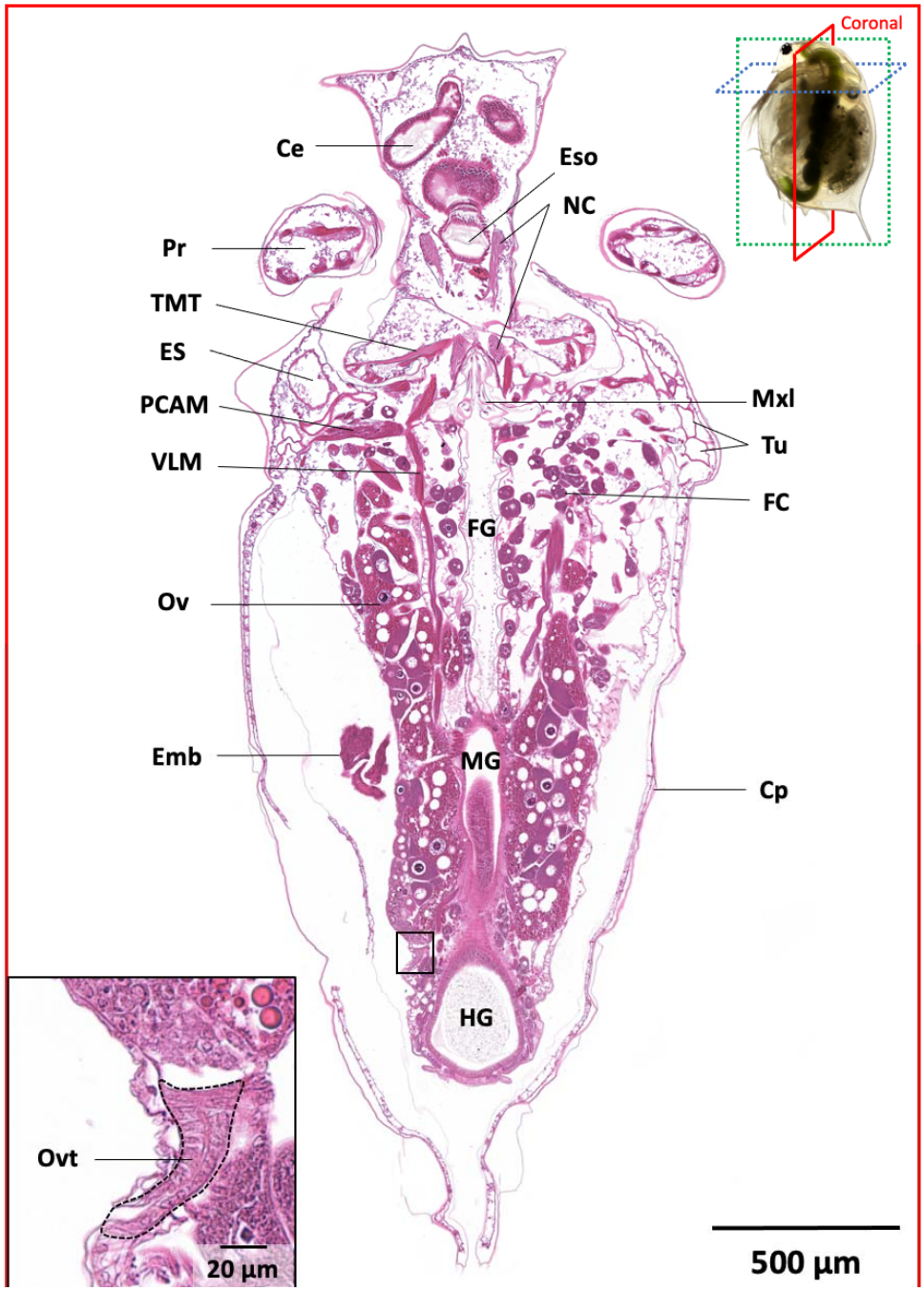

Figure 6. Representative image showing anatomical structures of female *D. magna* in the coronal plane. The coronal plane displays most of the structures in pairs, for example, the protopodites (Pr) of the swimming antennae, hepatic ceca (Ce), maxillules (Mxl), nerve cords (NC), transverse mandibular tendons (TMT), ovaries (Ov), and ventral longitudinal muscles (VLM). It also shows the food groove (FG) that channels food to the maxillules. Other features seen include the carapace (Cp), the end sac (ES) and tubules (Tu) of the maxillary gland, the midgut (MG), the abundant fat cells (FC), the hindgut (HG), and a portion of an embryo (Emb) in the brood chamber. Inset showing the oviduct (Ovt; dotted circle). Corresponding atlas link: https://daphnia.io/anatomy/histology/?t=coronal_female&z=10

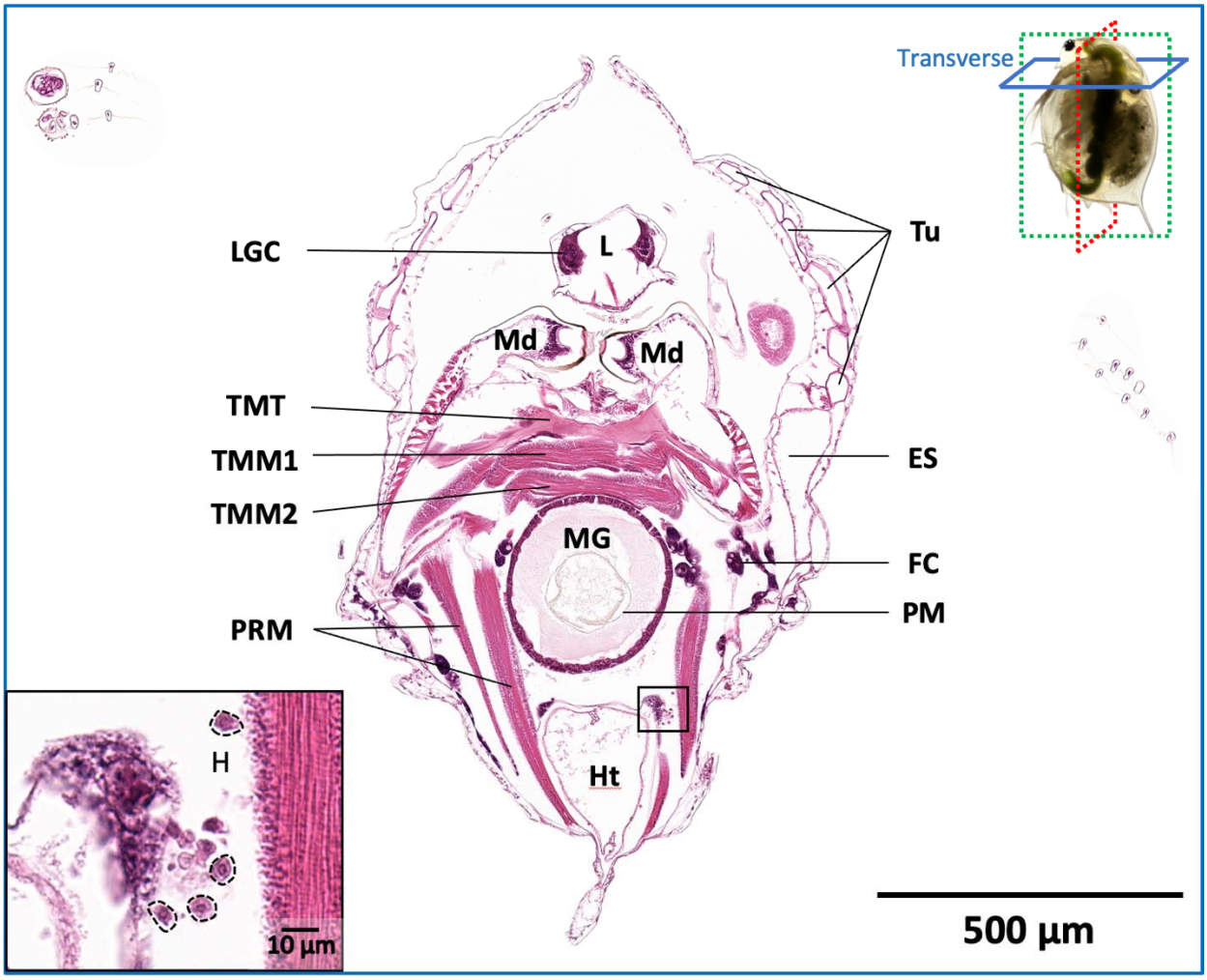

Figure 7. Representative image showing anatomical structures of female *D. magna* in the transverse plane. The transverse plane shows the asymmetrical paired mandibles (Md) with the transverse mandibular tendons (TMT), transverse mandibular muscles (TMM1), transverse muscles of mandibles (TMM2), and the posterior rotator muscles of mandibles (PRM). Other features seen include the labrum (L) that houses labral gland cells (LGC), end sac (ES) and tubules (Tu) of the maxillary gland, midgut (MG) with the peritrophic membrane (PM), and the heart (Ht). Inset displays several hemocytes (H) outlined by dotted circles.
Corresponding atlas link: http://daphnia.io/anatomy/histology/?t=transverse_female&z=10

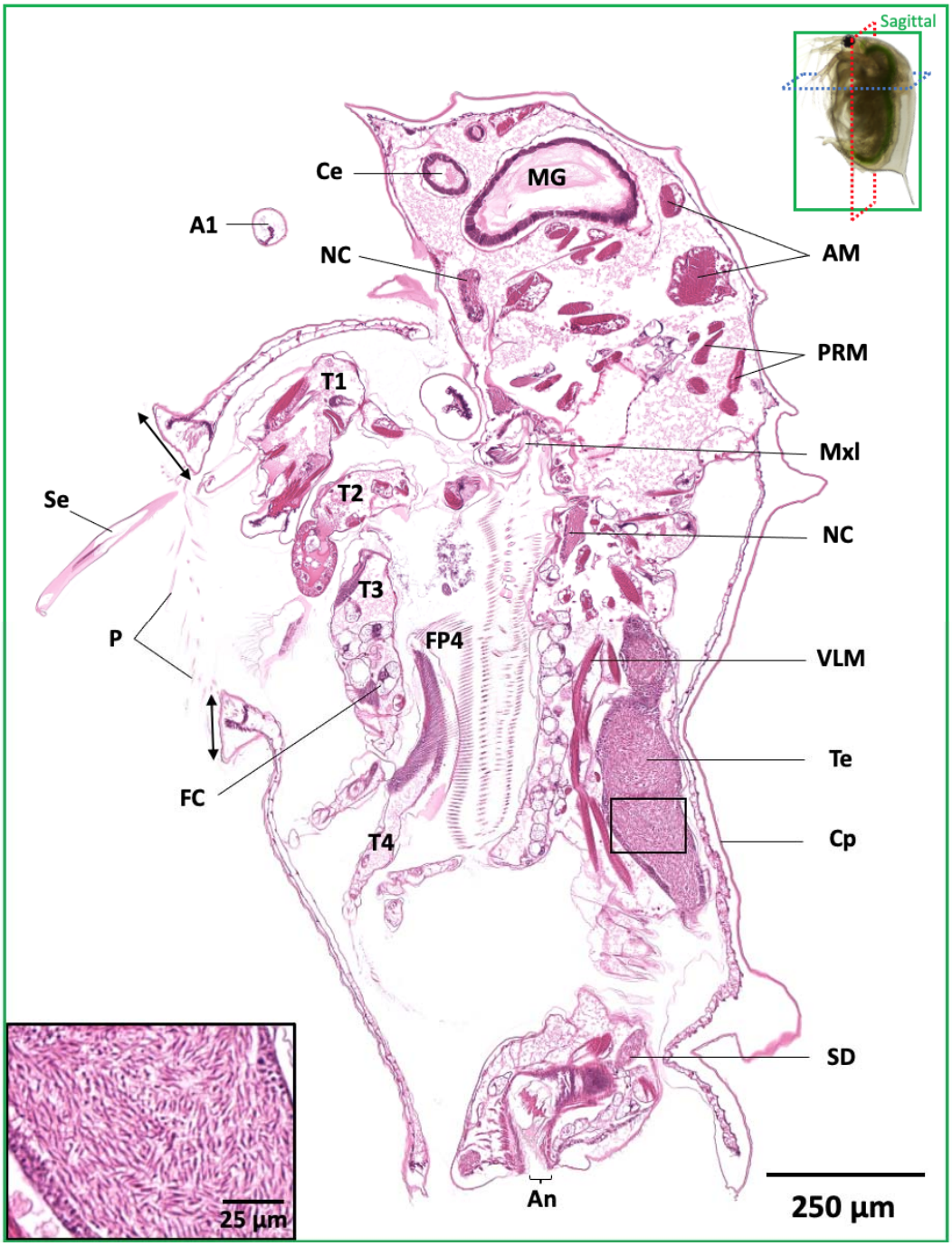

Figure 8. Representative image showing anatomical structures of male *D. magna* in the sagittal plane. The sagittal plane shows the elongated seta (Se) on the first thoracic limb, pubescence (P) at the wider ventral opening of the carapace, thickening of carapace at the ventral opening (arrows), one of the testes (Te), and a small portion of sperm duct (SD). Inset showing the spermatozoa in the testis. A1, antennule; A2M, antennal muscle; An, anus; Ce, hepatic cecum; Cp, carapace; ES, end sac of the maxillary gland; FC, fat cell; FP4, filter plate 4; Ht, heart; L, labrum; Md, mandible; MG, midgut; Mxl, maxillule; NC, nerve cord; PRM, posterior rotator muscle of mandible, T1-4, thoracic appendage 1-4; VLM, ventral longitudinal muscle. Corresponding atlas link: http://daphnia.io/anatomy/histology/?t=sagittal_male&z=3

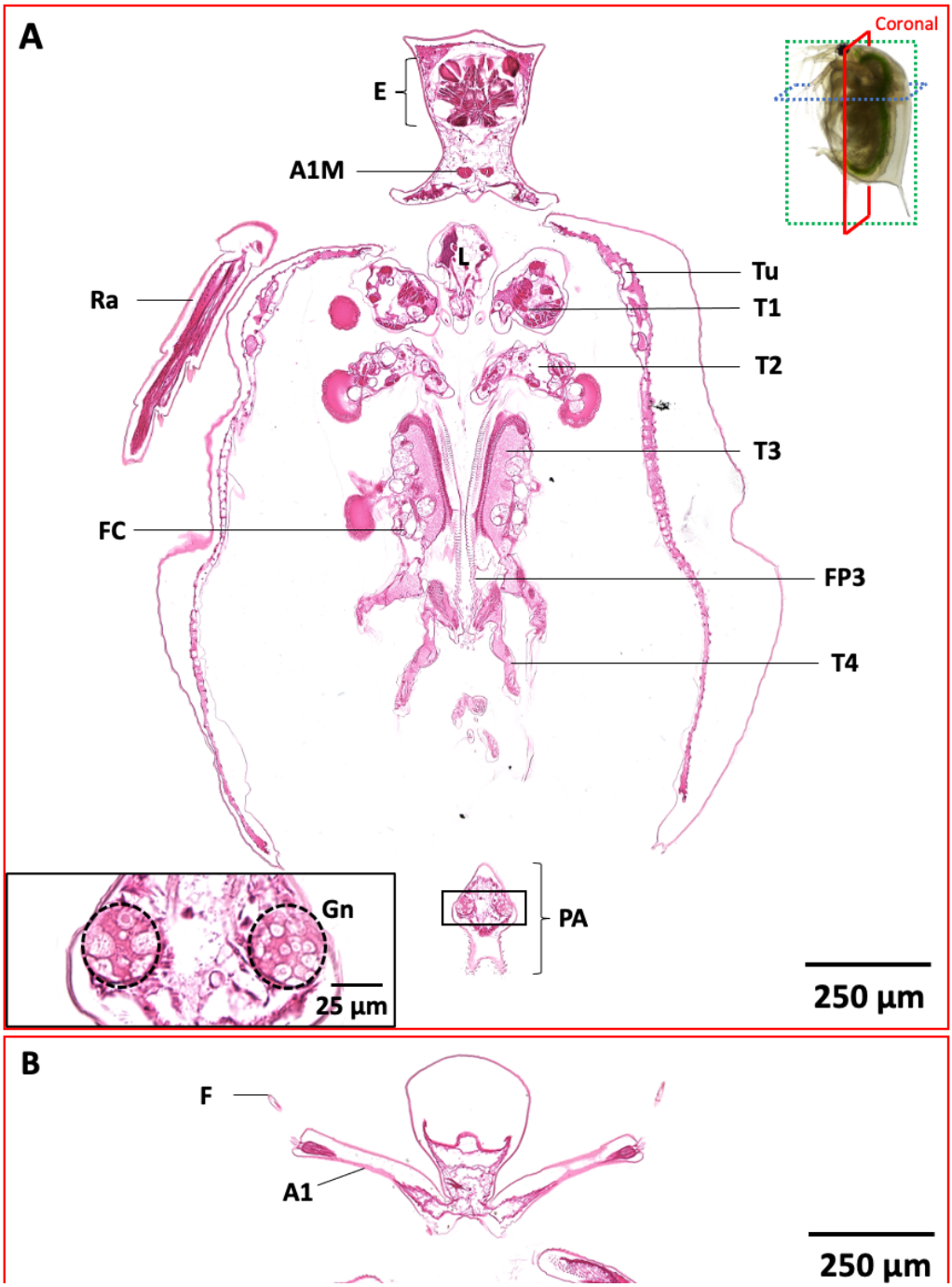

Figure 9. Representative images showing anatomical structures of male *D. magna* in the coronal plane. (A) This coronal section shows the antennule muscles (A1M) that are only present in the male, the first four paired thoracic limbs (T1-T4), and the gonopores (Gn, dotted circles in inset) on the postabdomen (PA). **(B)** This section, slightly ventral to panel A, displays the prominent and elongated antennules (A1) with flagella (F) at the tip. E, compound eye; FC, fat cell; FP3, filter plate 3; L, labrum; Ra, ramus of swimming antenna; Tu, tubule of the maxillary gland. Corresponding atlas links:
(A) https://daphnia.io/anatomy/histology/?t=coronal_male&z=4
(B) http://daphnia.io/anatomy/histology/?t=coronal_male&z=2&c=0.2,0.14,0.6,0.4

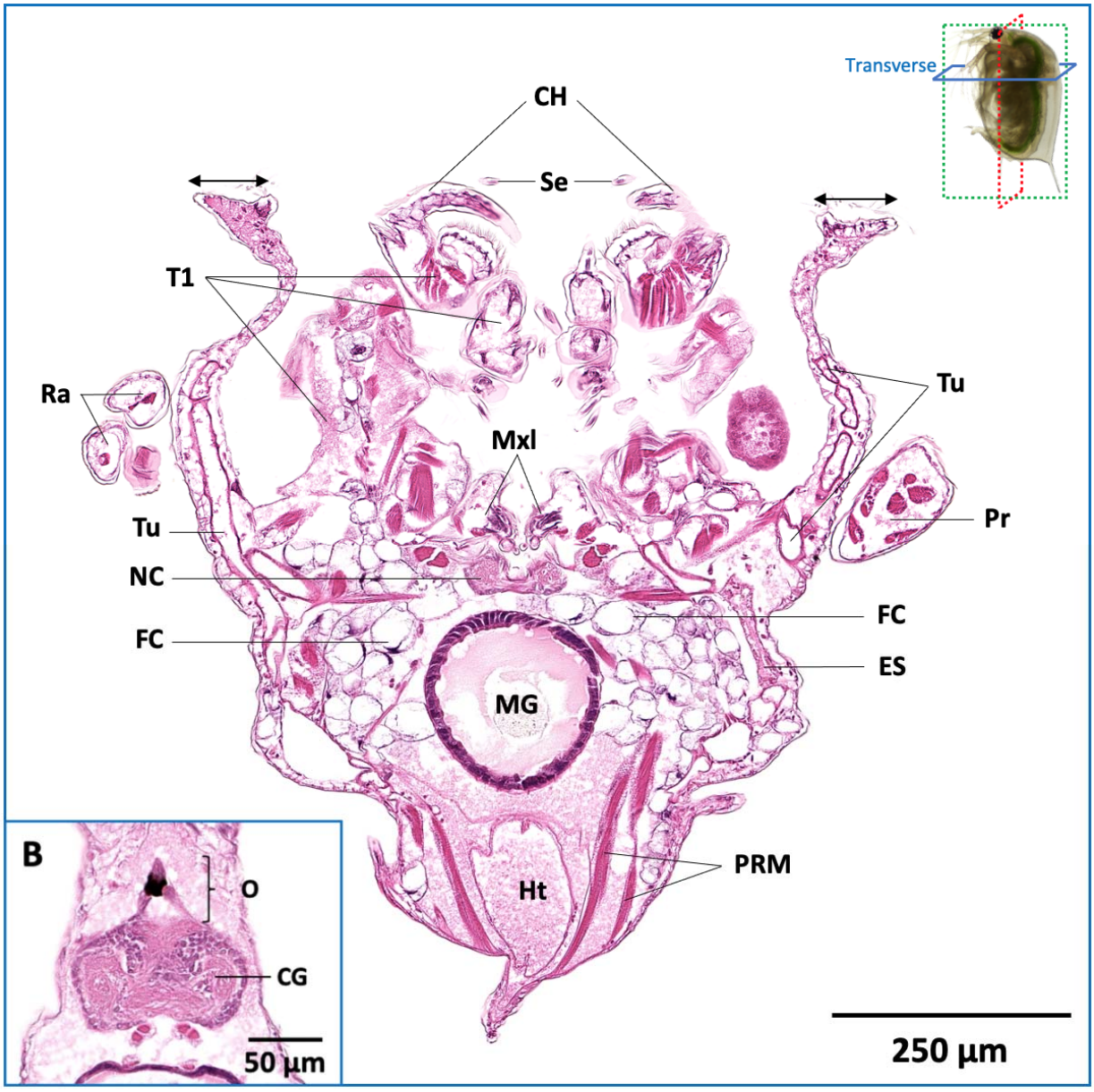

Figure 10. Representative image showing anatomical structures of male *D. magna* in the transverse plane. (A) This transverse section displays the paired copulatory hooks (CH) and elongated setae (Se) on the first thoracic limbs (T1), with pubescence and thickening of the carapace (arrows) at the ventral opening. This also shows the abundance of fat cells (FC) around the midgut (MG). Cp, carapace, ES, end sac of the maxillary gland; Ht, heart; L, labrum; Mxl, maxillule; NC, nerve cord; PRM, posterior rotator muscle of mandible; Pr, protopodite of swimming antenna; Ra, ramus of swimming antenna; Tu, tubule of the maxillary gland. **(B)** Pigmented ocellus (O) is shown to be connected to the cerebral ganglion (CG). This transverse section is slightly above that of panel A.

Corresponding atlas links:

(A) https://daphnia.io/anatomy/histology/?t=transverse_male&z=8

(B) http://daphnia.io/anatomy/histology/?t=transverse_male&z=4&c=0.43,0.25,0.18,0.12

Circulatory system

Daphnia have an open circulatory system and a myogenic heart (42,43). The heart (Ht) has a pair of ostia situated immediately to the anterior of the brood chamber, between the midgut and dorsal surface (Figures 5, 7, 9). As *Daphnia* are semi-transparent, the beating heart and the flow of hemolymph (blood) containing hemocytes (H) or blood cells (Figure 7 inset) can be easily observed (24,38) under low magnification.

Digestive system

Daphnia is filter feeders. Food particles are filtered through filter plates (FP3 and FP4) consisting of setae on thoracic limbs 3 and 4, passed through maxillules (Mxl) and mandibles (Md) to enter the esophagus (Eso), which is the first part of the digestive system (Figures 5). The digestive system also consists of paired hepatic ceca (Ce), midgut (MG), and hindgut (HG) (Figures 5, 6, 7, 8, and 10) that are lined with epithelial cells and microvilli, with the columnar epithelial cells in the midgut and cuboidal cells in hepatic ceca and hindgut (40,44). The labrum (L) houses labral gland cells (LGC) that have been suggested to be involved in food ingestion and endocrine function (48,49) (Figures 5, 7, and 9).

Excretory system

The maxillary gland, also known as the shell gland, is the organ of excretion of *Daphnia*, housed between the inner and outer walls of the carapace. It consists of an end sac (ES), a series of tubules (Tu), and an opening to the outside that is situated within the anterior part of the brood chamber (41) (Figures 6, 7, 9A, and 10A).

Locomotive and osmotic regulation

The second pair of antennae, also referred to as swimming antennae, is the primary organ of locomotion. Each swimming antenna has a protopodite (Pr), two rami (Ra) bearing setae (Se) (23) (Figure 6, 9A, 10A), and is supported by antennal muscles (A2M). *Daphnia* has five thoracic limbs (T1-T5) (26) (Figures 5, 8, and 9A). Movements of thoracic limbs produce a constant current that brings food particles into the digestive tract (25,51) and facilitates osmotic regulation, which occurs in the epipodite on each thoracic limb (35). First thoracic limbs in male

313 *Daphnia*, having elongated setae (Figure 8) and copulatory hooks (Figure 10A), are different
314 from those in the female.
315
316 ## Muscular system
317 The muscular system is very prominent and occupies a significant portion of the body. The
318 largest muscles are ventral and dorsal longitudinal muscles (VLM and DLM) that extend along
319 the gut, three paired antennal muscles (A2M), transverse mandibular muscles (TMM1),
320 transverse muscles of mandibles (TMM2), posterior rotator of the mandibles (PRM), carapace
321 adductor muscles (ACAM and PCAM) (Figures 5, 6, 7 and 8), and followed by groups of
322 muscles that allow the motion of thoracic limbs and postabdomen (27,51). Other small muscles
323 include those around the compound eye (27,29), labrum (27), and esophagus (27). All muscles
324 are striated and surrounded by sarcoplasm, which contains many nuclei and is mostly vacuolated.
325 Sarcoplasm is particularly abundant and more vacuolated in the antennal muscles.
326
327 ## Nervous, sensory, and vision system
328 *Daphnia* has a pigmented compound eye (E) consisting of 22 ommatidia, derived from two eyes
329 that fuse during embryonic development, and a small, pigmented ocellus (O) with three lens-like
330 bodies (Figure 10B). The optic nerve (ON) of each ommatidium forms a parallel bundle that
331 connects to the optic lobe of the cerebral ganglion (OL), which is then connected to the cerebral
332 ganglion (CG) (Figure 5). The cerebral ganglion is connected to two chains of nerve cords (NC)
333 that run along the thorax, underneath the gut, and reach other anatomical structures (36,37,45)
334 (Figures 6, 8 and 9).
335
336 ## Reproductive system
337 The ovaries in females (Figure 6) and the testes in males (Figure 8) are paired and situated
338 ventrally along the gut. *Daphnia* and all other species of the order Cladocera are cyclical
339 parthenogens, which involve both sexual (meiotic) and clonal (ameiotic) reproduction (52).
340 Under favorable environmental conditions, females reproduce parthenogenetically, and broods of
341 genetically identical embryos will develop in the brood chamber before being released. Sexual
342 reproduction is cued by environmental stress (often seasonal, including photoperiod,

343 temperature, and over-crowding) that triggers the production of genetically identical males
344 instead of females. During this sexual phase of the *Daphnia* life cycle, females also switch to
345 producing two haploid eggs. Unlike parthenogenetic embryos, the development of these sexually
346 produced embryos is arrested at the 3000-cell stage (53) and enter into a state of dormancy while
347 being encased within an ephippium that protects these embryos under diapause through harsh
348 environmental conditions for decades and even centuries (54,55). These two 'resting eggs' are
349 different from parthenogenetically produced eggs that can number up to 100 per brood.
350 Parthenogenetic eggs contain multiple oil droplets (od) of varying size and yolk granules (yg)
351 that are generally larger in size (34) (Figure 11).
352
353 Testes of male *Daphnia* consist of two long tubular structures connected to gonopores (Gn) or
354 ejaculatory openings by sperm ducts (Figure 8). Spermatogenesis begins at the testes' walls, and
355 mature spermatozoa are displaced inward toward the central region of the testes (46).
356
357 Fat cells, which are polyploid (56), consist of a massive portion of lipid and glycogen (47), are
358 abundant in healthy *Daphnia*. They are found along the gut, on the thoracic limbs, and around
359 ovaries or testes (Figures 5, 6, 7, 8, 9A, and 10A). These cells are most likely sites of the
360 vitellogenin synthesis (47). They have been implicated with epipodite cells (on thoracic limbs) in
361 the synthesis of hemoglobin (32).
362

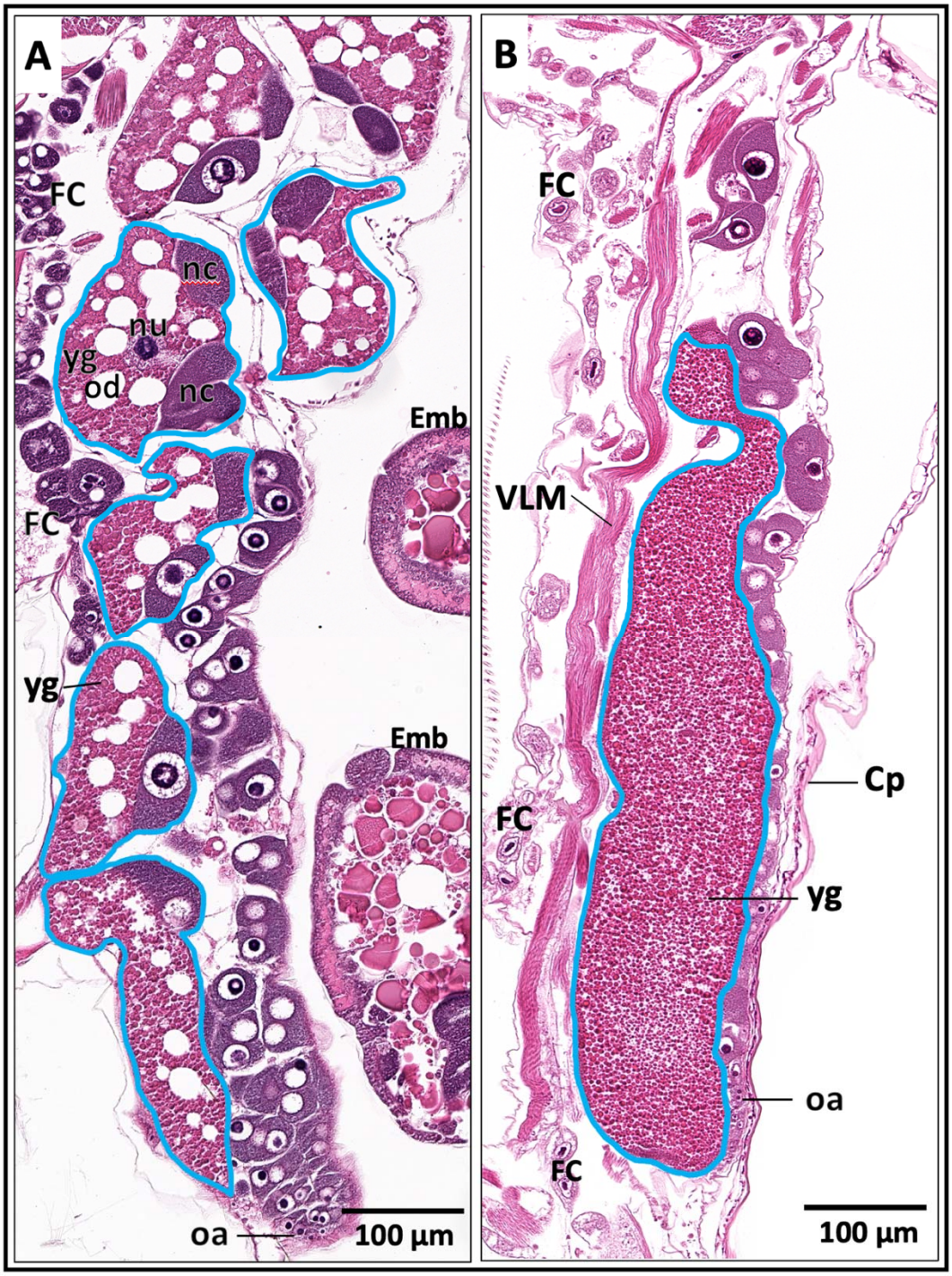

Figure 11. Comparison of ovarian eggs in females reproducing parthenogenetically or sexually. (A) The ovarian eggs of a female reproducing parthenogenetically contain a large amount of oil droplets (od) and yolk granules (yg) that are generally larger in size. **(B)** The ovarian egg of a female reproducing sexually contains a large proportion of fine yolk granules without oil droplets. Cp, carapace; Emb, embryo; FC, fat cell; nc, nurse cell; nu, the nucleus of oocyte; Oa, oogonia; VLM, ventral longitudinal muscle. A solid blue circle indicates an individual ovarian egg.

Sexual dimorphism in *Daphnia*

Due to the predominantly parthenogenetic life cycle of *Daphnia*, there is less information on male anatomy in contrast to the females. Our atlas provides the first detailed collection of histology images of male *Daphnia* that can contribute to the elucidation of sexual dimorphism in *Daphnia*. *Doublesex* genes *(Dsx1* and *Dsx2)* in *D. magna* had been reported to contribute to male sex determination and the development of male-specific structures (57–59). Time-lapse imaging (58) showed that most male-specific structures start developing during the early juvenile stage, except elongated antennules and the gonad. The male-specific expression had been detected in other anatomical structures, such as the compound eye (57) and skeletal muscles (58), of which sex difference has not been reported to date.

Sexual dimorphism in *Daphnia* includes smaller male body size and male prominence and elongation of antennules (A1), uniquely with flagella (F) at their tips (Figure 9B). Male antennules carry muscles (A1M) (Figure 9A) that are absent in the females. The first thoracic limbs of the males are equipped with elongated setae (Figure 8) and chitinized copulatory hooks (Figure 10A) that are used for clasping females during copulation. The male post-abdomen has gonopores (Figure 9A inset) that are involved in transferring mature spermatozoa from the testes to the female in the region of the oviduct during copulation. One of the male-specific traits illustrated in our atlas is that besides having a wider opening at the ventral margin of the carapace, thickened and angular margins (indicated by arrows in Figures 8, 10A, and 12) are observed around the hairy opening in males. We also show that fat cells in males are comparatively different from those in females as they contain much larger lipid droplets, reduced and less granular cytoplasm, and smaller nucleoli that are usually situated at the periphery of the cell (Figure 13). We hope the field of spatial biology will be assisted by this atlas to add insight into the role of gene regulation, proteins, and other molecules in physiological function in the morphogenesis of sexual dimorphism in *Daphnia*.

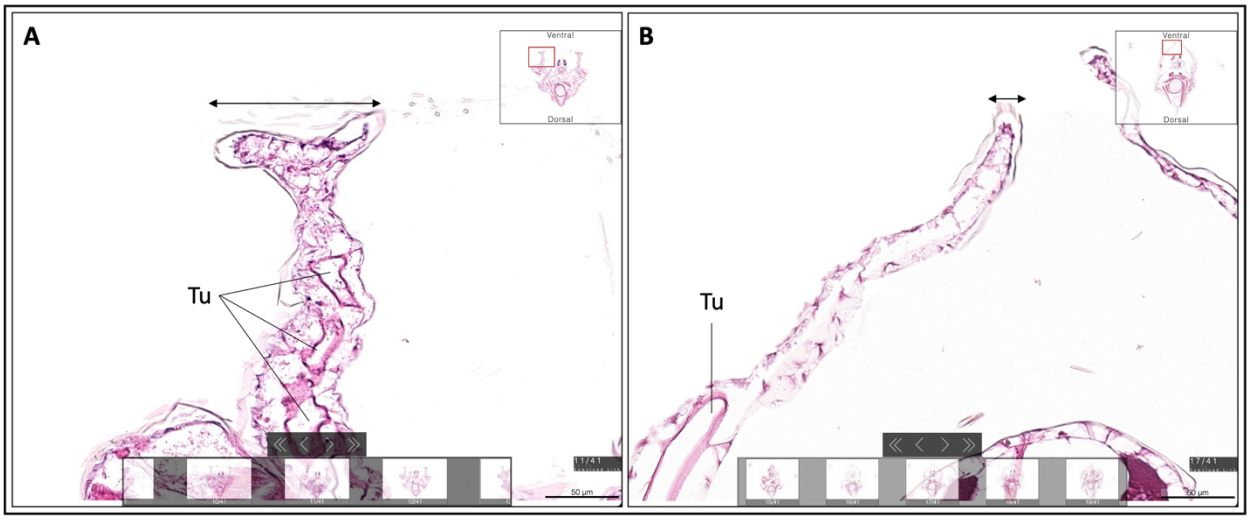

Figure 12. Comparison of male and female carapace at the ventral opening. (A) Thickening of the male carapace (arrow) at the ventral opening is shown as compared to that of the **(B)** female. Tu, Tubules of the maxillary gland. Corresponding atlas links:
(A) http://daphnia.io/anatomy/histology/?t=transverse_male_88&z=11&c=0.23,0.105,0.23,0.18
(B) http://daphnia.io/anatomy/histology/?t=transverse_female_57&z=17&c=0.36,0.07,0.20,0.15

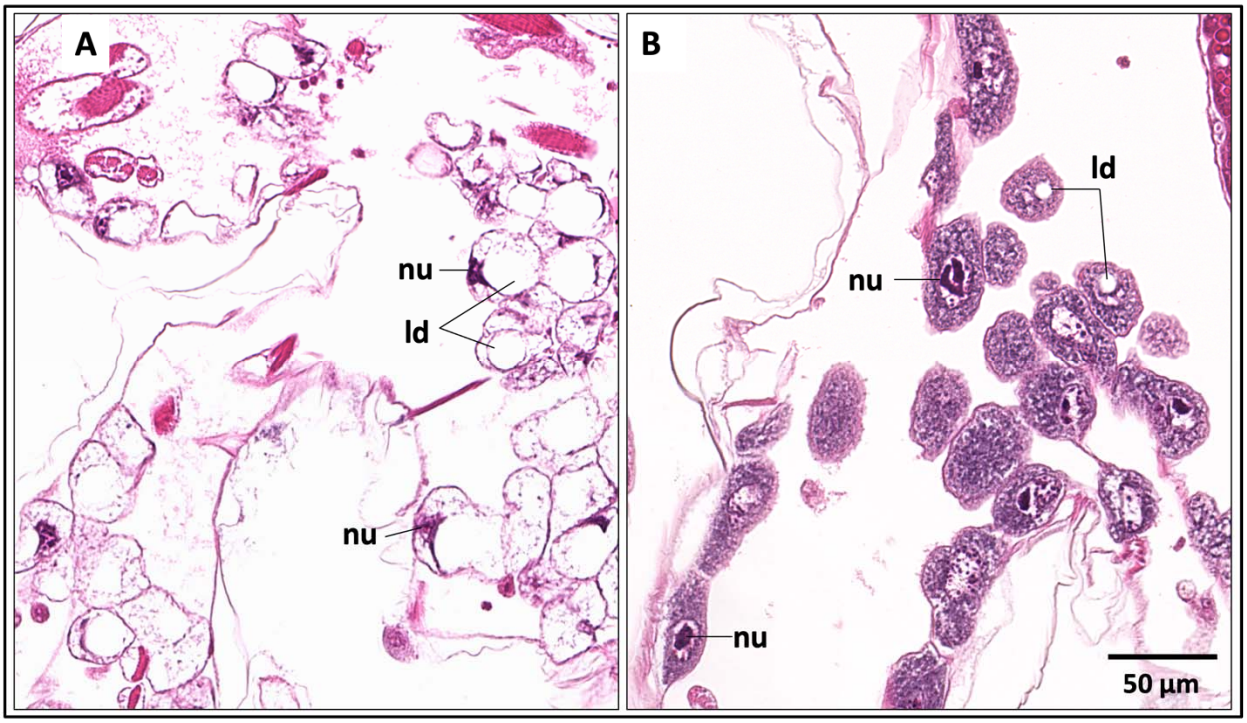

Figure 13. Comparison of male and female fat cells. (A) Fat cells in the male consist of larger lipid droplets (ld), reduced and less granular cytoplasm with smaller nucleoli (nu) that are situated at the cell periphery. **(B)** Fat cells in the female have more granular cytoplasm with smaller lipid droplets (ld) and bigger nucleoli (nu). Corresponding atlas links:
(A) http://daphnia.io/anatomy/histology/?t=sagittal_male&z=2&c=0.34,0.48,0.29,0.19
(B) http://daphnia.io/anatomy/histology/?t=sagittal_female&z=7&c=0.38,0.75,0.21,0.14

Conclusions and future direction

Atlases are foundational to the systematic characterization of anatomical (i.e., cellular and tissue) structures of organisms in both healthy and diseased states. DaHRA is created in recognition of *Daphnia* as a model organism for biology, especially toxicology and ecotoxicology that now includes extensive environmental genomics and metabolomics (5,11,12) but currently lacks correlation with microanatomical (histopathological) phenotypes. DaHRA provides the histological component of anatomical context for both sexes of *D. magna*, using a web-based interface that is far more accessible to the average user than traditional paper-based atlases. With DaHRA as a foundation for whole-organism evaluation, we anticipate the addition of pathological effects to the atlas for making the histological data more actionable in terms of hazard and/or risk assessment and regulatory decision-making for environmental health protection. Histopathological changes detected within a whole organism can be correlated with toxicological -omics data that require spatial context to understand and allow a more comprehensive understanding of toxicological effects across cell types, organ systems, and organisms. This integration of data is critical for discovering and applying adverse outcome pathways (60) for next-generation risk assessment (61) where there is no predetermined link between biomarkers of adversity, causative agents, and organ-specific effects. This will help to draw cause-effect relationships between environmental toxicants, tissue-specific adverse effects in sentinel and test organisms, and human and animal diseases associated with environmental toxicants.

DaHRA is envisioned to serve as a potential integrative platform for -omics data and to facilitate the addition of context from other imaging modalities. Molecular analyses including spatial transcriptomics (62), secondary ion mass spectrometry (63), and desorption electrospray ionization-mass spectrometry (64) typically rely on tissue histology to which the data can be mapped, and adding microanatomical context to molecular analyses has become a new priority. DaHRA can be used as a framework facilitating the addition of the -omics data. While 3D imaging modalities such as fluorescence-based confocal or laser sheet microscopy (65,66), or X-ray histotomography (67,68) provide the 3-dimensionality of anatomical structures that is lacking in histology, differential staining using a range of histochemical stains provides the basic understanding of tissue arrangement and cell identification that can be directly compared to the

grayscale characteristic of most 3D imaging modalities (69,70). Cross-referencing between 2D and 3D imaging modalities such as that illustrated in Figure 14 would enhance the utilization of both modalities. Notably, the understanding of structures from both 2D and 3D imaging modalities will require inspection of 2D images, which can benefit from our atlas labeling and visualization tools (Figure 14C). Using DaHRA as a reference for identifying tissue and cell types, 3D segmentation of anatomical structures is in progress and the creation of a *Daphnia* 3D atlas is underway.

Whole organism atlases are crucial for the elucidation of the anatomical and functional organization of tissues and organs. They are also essential as an integrative spatial framework for examining and identifying morphological and cellular change. The foundation for a whole-organism histology atlas is a representative set of high-resolution virtual slides (at least 40X magnification) encompassing a whole organism. The web-based platform allows the visualization and exploring of high-resolution virtual slides without requiring local file storage or downloading. Our platform also enables the interactive presentation of color-coded annotation of anatomical structures. The pipeline of DaHRA was designed with the intent to extend its features to the other model or sentinel organisms, which would be particularly exciting for creating cross-phylogenetic atlases.

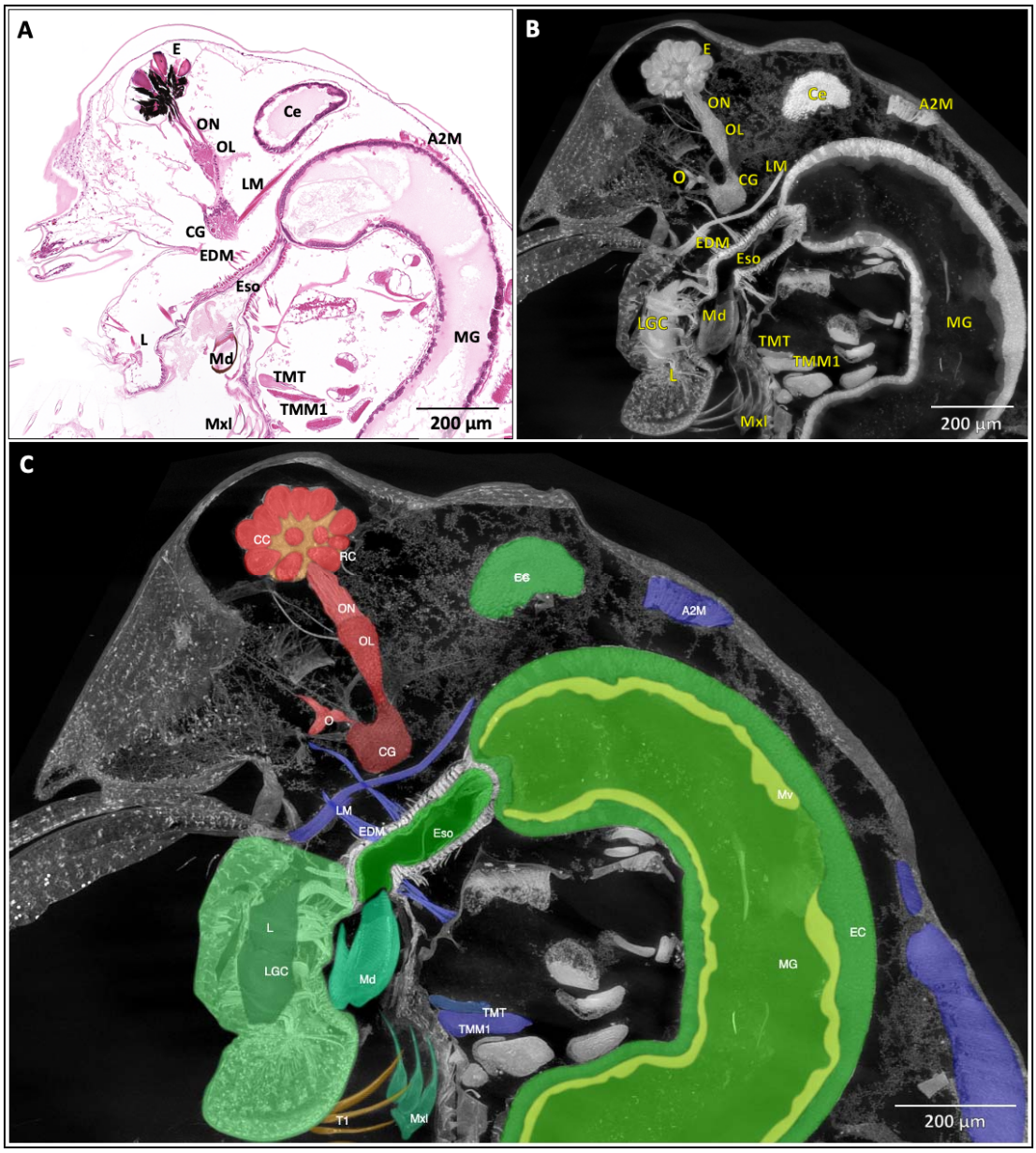

Figure 14. Cross-referencing of histology with microCT-based X-ray histotomography. (A) The anatomical structures of a female *D. magna* in a 5 µm histology section, cross-referenced to **(B)** a 25 µm stack from a histotomographic reconstruction of another female *D. magna* that provides more spatial context of various anatomical structures via easily adjustable stack thickness. Note that the connection of ocellus (O) to the cerebral ganglion (CG) and the 3-dimensionality of the compound eye (E) are demonstrated by the 25 µm histotomographic stack in panel B. **(C)** Color-overlay highlighting of the 25 µm stack shown in panel B, available in the atlas at http://daphnia.io/anatomy/histotomography/?t=AAA392&z=1&c=0.18,0.02,0.79,0.55. A2M, antennal muscle; Ce, hepatic cecum; CC, crystalline cone of ommatidium, EC, epithelial cell of midgut; EDM, esophageal dilator muscle; Eso, esophagus; L, labrum; LGC, labral gland cell; LM, levator muscle of labrum; Md, mandible; Mv, microvilli of midgut; Mxl, maxillule; MG, midgut; OL, optic lobe of cerebral ganglion; ON, optic nerve; TMM1, transverse mandibular muscle; TMT, transverse mandibular tendon.

Material and methods

Daphnia magna husbandry

Daphnia magna were purchased from Carolina Biological (NC, USA) and raised in "Aachener Daphnien-Medium" or ADaM (71) with modified content of selenium at room temperature (20°C ± 1°C) under a 16-hour light/8-hour dark photoperiod. *Daphnia magna* were fed three times weekly with 3.0 x 10^7 cells/ml of green microalgae (*Raphidocelis subcapitata)* and 0.1 mg/mL of dissolved bakers' yeast. The animal density was maintained at about 20 neonates, 10 juveniles and 5 to 7 reproducing adults per liter to prevent overcrowding and trigger the production of resting eggs and male *D. magna*. Under these conditions, animals reached maturity 6 to 8 days post-birth and reproduced parthenogenetically every 3 days with an average of 15 neonates per brood from the second brood onwards. Production of males and females carrying resting eggs was induced by overcrowding (>10 reproducing adults per liter) and shorter photoperiod (10 h).

Fixation and decalcification

Daphnia magna were euthanized in glass vials filled with bicarbonate water. Live *D. magna* were transferred using plastic transfer pipettes. Tips of transfer pipettes were trimmed at a 45° angle such that the diameter was double the size of the samples. Immediately following euthanasia, bicarbonate water was gently removed with a transfer pipette and replaced with at least 20X specimen volume of Bouin's solution (Newcomer Supply, WI) for fixation. The *D. magna* samples were immersed in fixative on a low-speed orbital shaker (Corning LSE) set to 55 revolutions per minute (RPM). We tested several fixatives and fixation parameters, such as duration and temperature listed in Table 1. After fixation in Bouin's solution, samples were washed twice using 1X phosphate-buffered saline (PBS) for 10 min each time. This was followed by decalcification in 20X sample volume of cold 6% formic acid (Sigma-Aldrich, MO) for 24 hours. Samples were then rinsed in 70% ethanol for one minute and immersed in fresh 70% ethanol for 30 min before agarose pre-embedding.

Table 1: Fixation parameters

Fixative	Fixation time and temperature	Decalcification by cold 6% formic acid time and temperature
Bouin's solution	48 h, 4 °C	24 h, 21 °C
	48 h, 21 °C	24 h, 21 °C
4% Paraformaldehyde	48 h, 4 °C	24 h, 4 °C
	48 h, 21 °C	24 h, 4 °C
10% Neutral buffered formalin	48 h, 4 °C	24 h, 4 °C
	48 h, 21 °C	24 h, 4 °C

Mold and agarose embedding

Samples were pre-embedded in 1% agarose block casted using "triangle mold" (Figure 1A-B) for histological processing following a protocol adapted from Sabaliauskas et al. (2006). After taping around the triangle mold, 2.5 mL of 1% agarose (Sigma-Aldrich, MO) at 55 °C were pipetted onto the mold, and then let solidify at room temperature (Figure 1C). Once solidified, the agarose block was removed gently from the mold (Figure 1D). Then, *D. magna* samples were transferred onto the agarose block using a plastic pipette. A thin layer of 70% ethanol was pipetted onto the block to help with the positioning of samples. Samples designated for the sagittal plane were laid on their sides with a swimming antenna in the wells and all rostra facing the same direction. Samples designated for coronal and transverse orientation were laid on their back in the wells (Figure 1 E-F). Once all the samples were positioned in individual wells, excess ethanol was carefully dried off using lint-free Kimwipes without agitating the samples. Each sample was first topped-off with one drop of molten 1% agarose (about 50 °C) without moving the sample, followed by a thin layer of 1% agarose covering all the samples. After the agarose solidified (~ 5 minutes at room temperature), the block was trimmed, placed into a tissue cassette, and stored in 70% ethanol for tissue processing. During paraffin embedding, the agarose blocks were positioned in the appropriate final orientation (transverse, sagittal or coronal) for sectioning.

Processing, sectioning, and staining

All samples were dehydrated and infiltrated in RMC Model 1530 automated closed reagent type tissue processor (Table 2). The *D. magna* samples were serially sectioned at 5 μm on a Leica RM2255 automated rotary microtome. Sections were then stained with Harris' hematoxylin and eosin (H&E) in an auto-stainer (Sakura Tissue Tek DRS 2000, IMEB, CA) following protocol adapted from Copper et al. (2018). The duration of hematoxylin staining was extended from 3 to 7 min to achieve better contrast for samples fixed with Bouin's solution (Table 3).

Table 2: Tissue Processing Steps

Duration	Solution	Temp (°C)	Vacuum (in. Hg)
45 min	80% Ethanol	25	15
45 min	95% Ethanol	25	15
1 hour	95% Ethanol	25	15
1 hour (repeat thrice)	100% Ethanol	25	15
1 hour (repeat twice)	Xylene	25	15
1 hour 30 min (repeat twice)	Paraffin	60	15
2 hours	Paraffin	60	15

Table 3: Automated staining steps

Time	Solution
3 min	Xylene
5 min	Xylene
2 min (repeat twice)	100% Ethanol
2 min	95% Ethanol
10 min	Tap water
7 min	Hematoxylin
1 min	Tap water
1 min	Acidified Alcohol
1 min	Tap water
0.2 min	Ammoniated water
1 min	Tap water
0.3 min	Eosin
1 min	30% Ethanol
1 min	95% Ethanol
1 min	100% Ethanol
1 min	Xylene

Histology slide digitization

All slides were scanned using an Aperio AT2 slide scanner (LeicaBiosystems, IL) and saved in TIFF format as digital slides. The regions of selected *D. magna* samples were then extracted using Image Scope. Three channels (Red, Green, Blue) of these digital slides were stacked using Fiji, oriented, and post-processed for background removal using Adobe Photoshop. Each set of digital slides was then pyramidally tiled (libvips) in preparation for the web-based viewer.

Labeling and segmentation workflow

For each anatomical structure included in the anatomical ontology (a list of terms organized by groups and subgroups, S3 File), we began by reviewing published literature, then concluding with a visual analysis of the structure in each of the three orthogonally cut histology slide sets. Anatomical structures included in the anatomical ontology were grouped and color-coded based on organ systems. Labeling and segmentation of anatomical structures were done one image at a time in Adobe Illustrator. The Adobe Illustrator Layer of an anatomical structure was first labeled corresponding to the appropriate ontological term. Each anatomical structure was segmented by outlining the structure with the curvature tool. Segmentation was then assigned the color based on the pre-determined color code. After completion of the labeling and segmentation of all anatomical structures on a given image, a single scalable vector graphic (SVG) was exported to be used as input for the web-based viewer.

Web-interface workflow

The file sizes associated with digital slides are on the order of >2 GB per slide, making scans challenging to view for users with standard computational resources. For easier access and usage of the data without the need to download full-resolution images, we developed an open-access, web-based digital slide viewing platform based on the open-access project OpenSeadragon (https://openseadragon.github.io/). This viewer combines annotations and digital scans into a seamless experience to provide user-friendly access to high-resolution data. The atlas' code was written in client-side JavaScript, HTML, and CSS requires no traditional download and has no server requirement to run the basic implementation. Pyramidally tiled images are parsed and visualized with OpenSeadragon. When the user loads a new image, the viewer opens the corresponding SVG file. The SVG file contains all the anatomical labels on a given image and

their corresponding shape vector information. The viewer parses all labels from the <g> element of the SVG file, plotting the corresponding regions on the viewer itself, and updates the ontology to note what regions are available to visualize on the current image.

Acknowledgments

The authors thank Patrick Leibich and the Department of Surgery, Penn State College of Medicine for 3D-SLA printing the casting molds, and Chadwick Harris and Debra Shearer for helping with histology sectioning and slide staining. The authors are grateful to Dr. Dula Parkison and Advanced Light Sources Beamline 8.3.2, Lawrence Berkeley National Labs for imaging the *Daphnia* samples. This work was supported by the National Institutes of Health (grant 1R24OD18559 to KCC), the Jake Gittlen Laboratories for Cancer Research, the Penn State Human Health and Environment Seed Grant supported by Pennsylvania Department of Health Commonwealth Universal Research Enhancement Program Grant. The Department of Health specifically disclaims responsibility for any analyses, interpretations, or conclusions. This work contributes to the PrecisionTox project that has received funding from the European Union's Horizon 2020 research and innovation program under grant agreement No 965406.

Competing Interests

The authors declare no competing interest.

References

1. Au DWT. The application of histo-cytopathological biomarkers in marine pollution monitoring: a review. Mar Pollut Bull. 2004 May 1;48(9):817–34.

2. Lampert W. Daphnia: Development of a Model Organism in Ecology and Evolution [Internet]. Book 21. Oldendorf/Luhe: International Ecology Institute; 2011 [cited 2022 Jan 21]. (Excellence in Ecology). Available from: https://www.semanticscholar.org/paper/Daphnia%3A-Development-of-a-Model-Organism-in-Ecology-Lampert/a373b75c3524f757e536ebaf49e5de393ca720d0

3. Stollewerk A. The water flea Daphnia - a "new" model system for ecology and evolution? J Biol. 2010 Jan 13;9(2):21.

4. Kikuchi M, Sasaki Y, Wakabayashi M. Screening of organophosphate insecticide pollution in water by using Daphnia magna. Ecotoxicol Environ Saf. 2000 Nov 1;47(3):239–45.

5. Tkaczyk A, Bownik A, Dudka J, Kowal K, Ślaska B. Daphnia magna model in the toxicity assessment of pharmaceuticals: A review. Sci Total Environ. 2021 Apr 1;763:143038.

6. Kühn R, Pattard M, Pernak K-D, Winter A. Results of the harmful effects of water pollutants to Daphnia magna in the 21 day reproduction test. Water Res. 1989 Apr 1;23(4):501–10.

7. Environmental Protection Agency. Ecological Effects Test Guidelines OCSPP850.1300: Daphnid chronic toxicity test. 1996.

8. Environmental Protection Agency. Methods for Measuring the Acute Toxicity of Effluents and Receiving Waters to Freshwater and Marine Organisms. 2002.

9. OECD. Test No. 202: Daphnia sp. Acute Immobilisation Test [Internet]. Paris: Organisation for Economic Co-operation and Development; 2004 [cited 2021 Nov 4]. Available from: https://www.oecd-ilibrary.org/environment/test-no-202-daphnia-sp-acute-immobilisation-test_9789264069947-en

10. OECD. Daphnia magna Reproduction Test (OECD TG 211) [Internet]. Paris: OECD; 2018 Sep [cited 2021 Nov 4] p. 253–63. Available from: https://www.oecd-ilibrary.org/environment/revised-guidance-document-150-on-standardised-test-guidelines-for-evaluating-chemicals-for-endocrine-disruption/daphnia-magna-reproduction-test-oecd-tg-211_9789264304741-12-en

11. Kim HJ, Koedrith P, Seo YR. Ecotoxicogenomic approaches for understanding molecular mechanisms of environmental chemical toxicity using aquatic invertebrate, Daphnia model organism. Int J Mol Sci. 2015 May 29;16(6):12261–87.

12. Shaw JR, Pfrender ME, Eads BD, Klaper R, Callaghan A, Sibly RM, et al. Daphnia as an emerging model for toxicological genomics. In: Hogstrand C, Kille P, editors. Advances in Experimental Biology [Internet]. Elsevier; 2008 [cited 2021 Oct 8]. p. 165–328. (Comparative Toxicogenomics; vol. 2). Available from: https://www.sciencedirect.com/science/article/pii/S1872242308000057

13. Bernet D, Schmidt H, Meier W, Burkhardt□Holm P, Wahli T. Histopathology in fish: proposal for a protocol to assess aquatic pollution. J Fish Dis. 1999;22(1):25–34.

14. Ramírez-Duarte W, Rondon Barragan I, Eslava-Mocha P. Acute toxicity and histopathological alterations of Roundup® herbicide on “cachama blanca” (Piaractus brachypomus). Pesqui Veterinária Bras. 2008 Nov 1;28:547.

15. Wester PW, Vos JG. Toxicological pathology in laboratory fish: an evaluation with two species and various environmental contaminants. Ecotoxicol Lond Engl. 1994 Mar;3(1):21–44.

16. Chakraborty S, Ray M, Ray S. Toxicity of sodium arsenite in the gill of an economically important mollusc of India. Fish Shellfish Immunol. 2010 Jul;29(1):136–48.

17. LaDouceur EEB, Wynne J, Garner MM, Nyaoke A, Keel MK. Lesions of Copper Toxicosis in Captive Marine Invertebrates With Comparisons to Normal Histology. Vet Pathol. 2016 May;53(3):648–58.

18. Kumar V, Abbas AK, Aster JC. Robbins & Cotran Pathologic Basis Of Disease (robbins Pathology) [Internet]. Tenth Edition. Elsevier; 2020 [cited 2022 Mar 28]. 1392 p. Available from: https://basi6direct.com/products/9780323531139

19. Treuting PM, Dintzis S, Montine KS, editors. Comparative Anatomy and Histology: A Mouse, Rat, and Human Atlas. 2nd edition. London San Diego Cambridge, MA Kidlington: Academic Press; 2017. 570 p.

20. Hebert PDN, Ward RD. Inheritance during parthenogenesis in Daphnia magna. Genetics. 1972 Aug;71(4):639–42.

21. Kvist J, Athanàsio CG, Pfrender ME, Brown JB, Colbourne JK, Mirbahai L. A comprehensive epigenomic analysis of phenotypically distinguishable, genetically identical female and male Daphnia pulex. BMC Genomics. 2020 Dec;21(1):17.

22. Copper JE, Budgeon LR, Foutz CA, van Rossum DB, Vanselow DJ, Hubley MJ, et al. Comparative analysis of fixation and embedding techniques for optimized histological preparation of zebrafish. Comp Biochem Physiol Toxicol Pharmacol CBP. 2018 Jun;208:38–46.

23. Agar WE. The swimming setae of Daphnia carinata. J Cell Sci. 1950 Dec 1;s3-91(16):353–68.

24. Auld SKJR, Scholefield JA, Little TJ. Genetic variation in the cellular response of Daphnia magna (Crustacea: Cladocera) to its bacterial parasite. Proc R Soc B Biol Sci. 2010 Nov 7;277(1698):3291–7.

25. Bednarska A. Adaptive changes in morphology of Daphnia filter appendages in response to food stress. Polish Journal of Ecology. 2006;54:663–8.

26. Benzie JAH. The Genus Daphnia (including Daphniopsis) (Anomopoda:Daphniidae). Kenobi Productions; 2005. 388 p.

27. Binder G. Das Muskelsystem von Daphnia. Int Rev Gesamten Hydrobiol Hydrogr. 1931;26(1–2):54–98.

28. Christensen AK, Owusu NG, Jean-Louis D. Carapace epithelia are rich in large filamentous actin bundles in Daphnia magna, Daphnia pulex, and Sida crystallina (Crustacea: Cladocera). Invertebr Biol. 2018;137(1):49–59.

29. Consi TR, Macagno ER, Necles N. The oculomotor system of Daphnia magna. The eye muscles and their motor neurons. Cell Tissue Res. 1987 Mar;247(3):515–23.

673 30. Ebert D. Introduction to Daphnia Biology [Internet]. Ecology, Epidemiology, and Evolution
674 of Parasitism in Daphnia [Internet]. National Center for Biotechnology Information (US);
675 2005 [cited 2022 Mar 31]. Available from: https://www.ncbi.nlm.nih.gov/books/NBK2042/

676 31. Edwards C. The anatomy of Daphnia mandibles. Trans Am Microsc Soc. 1980;99(1):2–24.

677 32. Goldmann T, Becher B, Wiedorn KH, Pirow R, Deutschbein ME, Vollmer E, et al. Epipodite
678 and fat cells as sites of hemoglobin synthesis in the branchiopod crustacean Daphnia
679 magna. Histochem Cell Biol. 1999 Nov;112(5):335–9.

680 33. Halcrow K. The fine structure of the carapace integument of Daphnia magna Straus
681 (Crustacea Branchiopoda). Cell Tissue Res. 1976 Jun 14;169(2):267–76.

682 34. Hiruta C, Tochinai S. Formation and structure of the ephippium (resting egg case) in relation
683 to molting and egg laying in the water flea Daphnia pulex De Geer (Cladocera:
684 Daphniidae). J Morphol. 2014 Jul;275(7):760–7.

685 35. Kikuchi S. The fine structure of the gill epithelium of a fresh-water flea, Daphnia magna
686 (Crustacea: Phyllopoda) and changes associated with acclimation to various salinities. I.
687 Normal fine structure. Cell Tissue Res. 1983;229(2):253–68.

688 36. Kress T, Harzsch S, Dircksen H. Neuroanatomy of the optic ganglia and central brain of the
689 water flea Daphnia magna (Crustacea, Cladocera). Cell Tissue Res. 2016 Mar
690 1;363(3):649–77.

691 37. McCoole MD, Baer KN, Christie AE. Histaminergic signaling in the central nervous system
692 of Daphnia and a role for it in the control of phototactic behavior. J Exp Biol. 2011 May
693 15;214(Pt 10):1773–82.

694 38. Metschnikoff E. A disease of Daphnia caused by a yeast. A contribution to the theory of
695 phagocytes as agents for attack on disease-causing organisms. Archiv Pathol Anat Physiol
696 Klin Med. 1884;96:177–95.

697 39. Rossi F. Comparative observations on the female reproductive system and parthenogenetic
698 oogenesis in Cladocera. Bolletino Zool. 1980 Jan;47(1–2):21–38.

699 40. Schultz TW, Kennedy JR. The fine structure of the digestive system of Daphnia pulex
700 (Crustacea: Cladocera). Tissue Cell. 1976 Jan 1;8(3):479–90.

701 41. Smirnov NN. Physiology of the Cladocera: Second Edition. Physiology of the Cladocera:
702 Second Edition. 2017. 1 p.

703 42. Stein RJ, Richter WR, Zussman RA, Brynjolfsson G. ULTRASTRUCTURAL
704 CHARACTERIZATION OF DAPHNIA HEART MUSCLE. J Cell Biol. 1966 Apr
705 1;29(1):168–70.

706 43. Steinsland AJ. Heart ultrastructure in Daphnia pulex De Geer (Crustacea, Branchiopoda,
707 Cladocera). J Crustac Biol. 1982;2(1):54–8.

708 44. Quaglia A, Sabelli B, Villani L. Studies on the intestine of Daphnidae (Crustacea, Cladocera)
709 ultrastructure of the midgut of Daphnia magna and Daphnia obtusa. J Morphol.
710 1976;150(3):711–25.

711 45. Weiss LC, Tollrian R, Herbert Z, Laforsch C. Morphology of the Daphnia nervous system: a
712 comparative study on Daphnia pulex, Daphnia lumholtzi, and Daphnia longicephala. J
713 Morphol. 2012 Dec;273(12):1392–405.

714 46. Wuerz M, Huebner E, Huebner J. The morphology of the male reproductive system,
715 spermatogenesis and the spermatozoon of Daphnia magna (Crustacea: Branchiopoda). J
716 Morphol. 2017 Nov;278(11):1536–50.

717 47. Zaffagnini F, Zeni C. Considerations on some cytological and ultrastructural observations on
718 fat cells of Daphnia (Crustacea, Cladocera). Bollettino di zoologia. 1986;53(1):33–9.

719 48. Zaffagnini F, Zeni C. Ultrastructural investigations on the labral glands of Daphnia obtusa
720 (Crustacea, Cladocera). J Morphol. 1987 Jul;193(1):23–33.

721 49. Zeni C, Franchini A. A preliminary histochemical study on the labral glands of Daphnia
722 obtusa (Crustacea, Cladocera). Acta Histochem. 1990;88:175–81.

723 50. Smirnov NN. Physiology of the Cladocera. Physiol Cladocera. 2013 Oct 1;1–336.

724 51. Fryer G. Functional morphology and the adaptive radiation of the Daphniidae
725 (Branchiopoda: Anomopoda). Philos Trans R Soc Lond B Biol Sci. 1991 Jan
726 29;331(1259):1–99.

727 52. Decaestecker E, De Meester L, Mergeay J. Cyclical parthenogenesis in Daphnia: sexual
728 versus asexual reproduction. In: Schön I, Martens K, Dijk P, editors. Lost Sex: The
729 Evolutionary Biology of Parthenogenesis [Internet]. Dordrecht: Springer Netherlands; 2009
730 [cited 2022 Jan 21]. p. 295–316. Available from: https://doi.org/10.1007/978-90-481-2770-
731 2_15

732 53. Chen L, Barnett RE, Horstmann M, Bamberger V, Heberle L, Krebs N, et al. Mitotic activity
733 patterns and cytoskeletal changes throughout the progression of diapause developmental
734 program in Daphnia. BMC Cell Biol. 2018 Dec 29;19:30.

735 54. Cáceres CE. Interspecific variation in the abundance, production, and emergence of Daphnia
736 diapausing eggs. Ecology. 1998;79(5):1699–710.

737 55. Mergeay J, Verschuren D, Kerckhoven LV, Meester LD. Two hundred years of a diverse
738 Daphnia community in Lake Naivasha (Kenya): effects of natural and human-induced
739 environmental changes. Freshw Biol. 2004;49(8):998–1013.

740 56. Beaton MJ, Hebert PDN. Miniature genomes and endopolyploidy in cladoceran crustaceans.
741 Genome. 1989 Dec 1;32(6):1048–53.

742 57. Kato Y, Kobayashi K, Watanabe H, Iguchi T. Environmental Sex Determination in the
743 Branchiopod Crustacean Daphnia magna: Deep Conservation of a Doublesex Gene in the
744 Sex-Determining Pathway. PLoS Genet [Internet]. 2011 Mar 24 [cited 2021 Mar 23];7(3).
745 Available from: https://www.ncbi.nlm.nih.gov/pmc/articles/PMC3063754/

746 58. Nong QD, Mohamad Ishak NS, Matsuura T, Kato Y, Watanabe H. Mapping the expression
747 of the sex determining factor Doublesex1 in Daphnia magna using a knock-in reporter. Sci
748 Rep. 2017 Nov 2;7(1):13521.

749 59. Wuerz M, Whyard S, Loadman NL, Wiegand MD, Huebner JD. Sex determination and gene
750 expression in Daphnia magna exposed to juvenile hormone. J Plankton Res. 2019 Jul
751 26;41(4):393–406.

752 60. OECD. Adverse Outcome Pathways, Molecular Screening and Toxicogenomics - OECD
753 [Internet]. 2022 [cited 2022 Feb 22]. Available from:
754 https://www.oecd.org/chemicalsafety/testing/adverse-outcome-pathways-molecular-
755 screening-and-toxicogenomics.htm

756 61. US EPA. Next Generation Risk Assessment: incorporation of recent advances in molecular,
757 computational, and systems biology (final report) [Internet]. 2014 [cited 2022 Feb 22].
758 Available from: https://cfpub.epa.gov/ncea/risk/recordisplay.cfm?deid=286690

759 62. Marx V. Method of the Year: spatially resolved transcriptomics. Nat Methods. 2021
760 Jan;18(1):9–14.

761 63. Bonnin EA, Rizzoli SO. Novel secondary ion mass spectrometry methods for the
762 examination of metabolic effects at the cellular and subcellular levels. Front Behav
763 Neurosci. 2020;14:124.

764 64. Smith MJ, Weber RJM, Viant MR. Spatially mapping the baseline and Bisphenol-A exposed
765 Daphnia magna lipidome using desorption electrospray ionization-mass spectrometry.
766 Metabolites. 2022 Jan;12(1):33.

767 65. Connelly SJ, Walling K, Wilbert SA, Catlin DM, Monaghan CE, Hlynchuk S, et al. UV-
768 Stressed Daphnia pulex increase fitness through uptake of Vitamin D3. PLOS ONE. 2015
769 Jul 6;10(7):e0131847.

770 66. Mittmann B, Ungerer P, Klann M, Stollewerk A, Wolff C. Development and staging of the
771 water flea Daphnia magna (Straus, 1820; Cladocera, Daphniidae) based on morphological
772 landmarks. EvoDevo. 2014 Mar 18;5(1):12.

773 67. Ding Y, Vanselow DJ, Yakovlev MA, Katz SR, Lin AY, Clark DP, et al. Computational 3D
774 histological phenotyping of whole zebrafish by X-ray histotomography. White RM, Stainier
775 DY, Ekker SC, editors. eLife. 2019 May 7;8:e44898.

776 68. Yakovlev MA, Vanselow DJ, Ngu MS, Zaino CR, Katz SR, Ding Y, et al. A wide-field
777 micro-computed tomography detector: micron resolution at half-centimetre scale. J

778 Synchrotron Radiat [Internet]. 2022 Mar 1 [cited 2022 Feb 22];29(2). Available from:
779 https://journals.iucr.org/s/issues/2022/02/00/mo5248/

780 69. Castejón D, Alba-Tercedor J, Rotllant G, Ribes E, Durfort M, Guerao G. Micro-computed
781 tomography and histology to explore internal morphology in decapod larvae. Sci Rep. 2018
782 Sep 26;8(1):14399.

783 70. Schulz G, Waschkies C, Pfeiffer F, Zanette I, Weitkamp T, David C, et al. Multimodal
784 imaging of human cerebellum - merging X-ray phase microtomography, magnetic
785 resonance microscopy and histology. Sci Rep. 2012 Nov 9;2(1):826.

786 71. Klüttgen B, Dülmer U, Engels M, Ratte HT. ADaM, an artificial freshwater for the culture of
787 zooplankton. Water Res. 1994 Mar 1;28(3):743–6.

788 72. Sabaliauskas NA, Foutz CA, Mest JR, Budgeon LR, Sidor AT, Gershenson JA, et al. High-
789 throughput zebrafish histology. Methods. 2006 Jul 1;39(3):246–54.

790 73. OpenSeadragon [Internet]. [cited 2021 Dec 15]. Available from:
791 https://openseadragon.github.io/

792 74. Haney JF, Hall DJ. Sugar-coated Daphnia: A preservation technique for Cladocera1. Limnol
793 Oceanogr. 1973;18(2):331–3.

794